

Special Section:

One Health, Microbes, and Climate Change

Xiaoning Wang and Xin Sui contributed equally to this work and share first authorship.

Key Points:

- The NLRP3 inflammasome potentially contributes to cytotoxicity induced by six types of OPPs
- Inhibition of the NLRP3 pathway effectively prevented cytotoxicity caused by six OPPs
- The study proposed targets for broad-spectrum antitoxic drugs to prevent OPPs-poisoning

Supporting Information:

Supporting Information may be found in the online version of this article.

Correspondence to:

T. Zhu, Y. Luo and Y. Wang, tongzhu@mail.neu.edu.cn; luoyuan2006@163.com; yonganw@126.com

Citation:

Wang, X., Sui, X., Sun, Y., Cui, Z., Ma, N., Wang, S., et al. (2024). Potential common mechanisms of cytotoxicity induced by organophosphorus pesticides via NLRP3 inflammasome activation. *GeoHealth*, 8, e2023GH000888. <https://doi.org/10.1029/2023GH000888>

Received 5 JULY 2023

Accepted 30 MAR 2024

Author Contributions:

Conceptualization: Xiaoning Wang, Xin Sui, Tong Zhu, Yuan Luo, Yongan Wang

Formal analysis: Ziqi Cui

Funding acquisition: Tong Zhu, Yuan Luo, Yongan Wang

© 2024 The Authors. GeoHealth published by Wiley Periodicals LLC on behalf of American Geophysical Union.

This is an open access article under the terms of the Creative Commons Attribution-NonCommercial License, which permits use, distribution and reproduction in any medium, provided the original work is properly cited and is not used for commercial purposes.



Potential Common Mechanisms of Cytotoxicity Induced by Organophosphorus Pesticides via NLRP3 Inflammasome Activation

Xiaoning Wang^{1,2}, Xin Sui², Yangyang Sun², Ziqi Cui², Ning Ma³, Shuai Wang², Jun Yang², Fengying Liu², Weijie Yang², Zhenyu Xiao², Tong Zhu¹ , Yuan Luo² , and Yongan Wang²

¹School of Mechanical Engineering and Automation, Institute of Process Equipment and Environmental Engineering, Northeastern University, Shenyang, China, ²State Key Laboratory of Toxicology and Medical Countermeasures, Beijing Institute of Pharmacology and Toxicology, Beijing, China, ³900TH Hospital of Joint Logistics Support Force, Fuzhou, China

Abstract The Multi-Threat Medical Countermeasure (MTMC) technique is crucial for developing common biochemical signaling pathways, molecular mediators, and cellular processes. This study revealed that the Nod-like receptor 3 (NLRP3) inflammasome pathway may be a significant contributor to the cytotoxicity induced by various organophosphorus pesticides (OPPs). The study demonstrated that exposure to six different types of OPPs (paraoxon, dichlorvos, fenthion, dipterex, dibrom, and dimethoate) led to significant cytotoxicity in BV2 cells, which was accompanied by increased expression of NLRP3 inflammasome complexes (NLRP3, ASC, Caspase-1) and downstream inflammatory cytokines (IL-1 β , IL-18), in which the order of cytotoxicity was dichlorvos > dipterex > dibrom > paraoxon > fenthion > dimethoate, based on the IC₅₀ values of 274, 410, 551, 585, 2,158, and 1,527,566 μ M, respectively. The findings suggest that targeting the NLRP3 inflammasome pathway could be a potential approach for developing broad-spectrum antitoxic drugs to combat multi-OPPs-induced toxicity. Moreover, inhibition of NLRP3 efficiently protected the cells against cytotoxicity induced by these six OPPs, and the expression of NLRP3, ASC, Caspase-1, IL-1 β , and IL-18 decreased accordingly. The order of NLRP3 affinity for OPPs was dimethoate > paraoxon > dichlorvos > dibrom > (fenthion and dipterex) based on K_D values of 89.8, 325, 1,460, and 2,690 μ M, respectively. Furthermore, the common molecular mechanism of NLRP3-OPPs was clarified by the presence of toxicity effector groups (benzene ring, nitrogen/oxygen-containing functional group); =O, -O-, or =S (active) groups; and combination residues (Gly271, Asp272). This finding provided valuable insights into exploring the common mechanisms of multiple threats and developing effective therapeutic strategies to prevent OPPs poisoning.

Plain Language Summary This study aimed to explore the role of Nod-like receptor 3 (NLRP3) inflammasome activation in organophosphorus pesticide (OPPs)-induced cytotoxicity. Six different OPPs, including dimethoate, paraoxon, dichlorvos, dibrom, fenthion, and dipterex, were introduced to BV2 cells and caused significant cytotoxicity along with increased expression of NLRP3 inflammasome complexes and downstream cytokines. Inversely, inhibition of NLRP3 protected against these OPPs. We believe that our study makes a significant contribution to the literature because it suggests that the NLRP3 inflammasome pathway may be a common mechanism of multi-OPPs-induced cytotoxicity. By introducing a therapeutic target for OPPs poisoning prevention, broad-spectrum antitoxic drugs may be designed to effectively protect against OPPs-induced cytotoxicity.

1. Introduction

Organophosphorus pesticides (OPPs) are widely used in agriculture and can pose a significant risk to public health and ecological security due to their high-enrichment levels and ability to migrate and accumulate in the environment. Examples of OPPs include paraoxon, dichlorvos, fenthion, dipterex, dibrom, and dimethoate, and so on (Bharate et al., 2010; Hu & Yang, 2020; Pundir et al., 2019). These compounds can cause neurological damage, as well as acute and chronic toxic effects on the immune system due to their teratogenic and mutagenic properties (Grout et al., 2020; Javeres et al., 2021; Yao et al., 2020). As a result, they have sparked interest among toxicologists and environmental scientists and remain a pressing concern due to their continuing use and unknown toxicities. While there is limited data on the confusion of signaling pathways or varied inflammatory pathologies caused by different countermeasures used to combat OPPs poisoning, many patients are hospitalized owing to the

Investigation: Xiaoning Wang, Xin Sui, Yangyang Sun, Ziqi Cui, Ning Ma, Shuai Wang, Fengying Liu, Zhenyu Xiao

Methodology: Xiaoning Wang, Xin Sui, Yangyang Sun

Project administration: Tong Zhu, Yuan Luo, Yongan Wang

Resources: Tong Zhu, Yuan Luo, Yongan Wang

Supervision: Tong Zhu, Yuan Luo, Yongan Wang

Validation: Jun Yang

Visualization: Weijie Yang

Writing – original draft: Xiaoning Wang

Writing – review & editing: Tong Zhu, Yuan Luo, Yongan Wang

improper use of OPPs, and there currently exist no specific drug therapies for these patients (Fernandes et al., 2015; González-González et al., 2018).

The primary mechanism of action for organophosphorus insecticides is neurotoxicity. Once they get into the body, OPPs can easily bind to the active site of acetylcholinesterase, forming phosphocreatine cholinesterase. This leads to the inactivation of acetylcholinesterase and the subsequent acetylcholine accumulation in the body, interfering with normal nerve conduction and ultimately inducing cholinergic syndrome, which can lead to symptoms such as convulsions, muscle tremors. In addition to the cholinergic system, recent research suggests that inflammation may also play a role in secondary brain injury induced by convulsions, ultimately resulting in chronic mental disorders and delayed polyneuropathy (Cowan et al., 2004). Studies have found that organophosphorus compounds can cause a cellular inflammatory response *through the* activated microglial, leading to increased levels of neuroinflammatory genes such as IL-1 β and IL-18 (Zimmer et al., 1997). However, the specific biochemical processes involved in this inflammatory response and the mechanisms underlying the activation of microglial cells remain unclear and require further investigation.

Inflammations are cytoplasmic supermolecular complexes that are activated in response to exogenous chemical invasions or endogenous damage signals, the activation of inflammatory and resulting inflammation can lead to negative health outcomes, such as neuroinflammation and neurodegenerative diseases (Elliott & Sutterwala, 2015; M. Liu et al., 2021; Martinon et al., 2002). The inflammatory response induced by toxicants via Nod-like receptor 3 (NLRP3)/Caspase-1/ASC-dependent mechanisms results in triggered cellular cascade events or pyroptosis, with the release of IL-1 β and IL-18 (Eychenne et al., 2022; X. D. Liu et al., 2023; Martín et al., 2017; S. Wang et al., 2021; X. N. Wang et al., 2021). The NLRP3 inflammasome can be assembled and activated by electrophilic compounds like cholesterol, trimethyltin, acrylamide, and sevoflurane through the NACHT or leucine-rich repeats (LRR) domain (Duewell et al., 2010; Long et al., 2019; Sharif et al., 2019; Sui et al., 2020; Zhu et al., 2023). Organophosphate paraoxon, a classic electrophilic compound, could activate the intracellular NLRP3/Caspase-1 pathway, which enhance Caspase-1 expression, increase the inflammatory response in brain cells, causes central nervous system (CNS) injury, and weakens the blood-brain barrier endothelium by attenuating junction protein expression, which could lead to decreased barrier integrity (Israelov et al., 2020). Thus, the NLRP3 inflammasome is a potential target of various organophosphorus pesticides, identifying ways to modulate NLRP3 activity may lead to new strategies for mitigating the harmful effects of environmental toxins and other damage signals.

The “Multi-Threat Medical Countermeasure (MTMC)” hypothesis proposes a different approach to drug discovery that is more suitable for the increasing number of toxicants that we were exposed. Rather than developing specific countermeasures against individual toxins, the goal is to identify common mechanisms that underlie multiple toxicities and use this information to develop a single broad-spectrum countermeasure drug (Caruso et al., 2020). In the case of OPPs, this study aims to investigate the common mechanisms between different types of OPPs and the NLRP3 inflammasome. By understanding these mechanisms, it may be possible to develop a single drug that can effectively counteract the harmful effects of a range of OPPs. This approach is more efficient and cost-effective than developing multiple specific countermeasures for each individual pesticide (Cowan et al., 2005; Throckmorton et al., 2020). Key areas of focus include the study of OPPs, the development of bioengineering and biomarkers, the association between environmental exposure and epigenetics, the investigation of pollutant accumulation and mixture toxicity, as well as the advancement of risk assessment and management strategies (Hsu et al., 2023; Sato et al., 2021). Additionally, new areas of research such as toxicology, bioaccumulation and biomagnification effects, environmental justice, and societal impacts have emerged (Sato et al., 2021; N. Zhang et al., 2021). These advancements contribute to a better understanding of the complex interactions between pollutants and the environment, ultimately leading to the protection of human and ecological health.

2. Material and Methods

2.1. Chemicals

Six kinds of OPPs, including paraoxon, dichlorvos, fenthion, dipterex, dibrom, and dimethoate, were purchased from Shanghai Aladdin Biochemical Technology Co., Ltd. (Shanghai, China). The NLRP3 inflammasome inhibitor, MCC950, was purchased from Selleck Biotechnology Co., Ltd. (Houston, TX, USA). Cell Counting Kit-8 (CCK-8) and Cytotoxicity LDH Assay Kit-WST were obtained from Dojindo Laboratories (Kumamoto, Japan).

Enzyme-linked immunosorbent assay (ELISA) kits were purchased from Abcam (Cambridge, UK). PrimeScript RT reagent kit with gDNA Eraser and TB Green Premix Ex Taq II was purchased from Takara Bio, Inc. (Kusatsu, Japan). The hNLRP3 LRR recombinant protein was obtained from ImmunoClone Biosciences Co., Ltd. (Huntington Station, NY, USA).

2.2. Cell Cultures and Treatment

BV2 microglial cells were supplied by the Cell Resource Center, Institute of Basic Medicine, Chinese Academy of Medical Sciences (Beijing, China), and cultured in Dulbecco's Modified Eagle Medium (DMEM) containing 10% fetal bovine serum. BV2 cells (5×10^4 cells/mL) were seeded in 96-well (100 μ L/well) and 6-well (2 mL/well) plates and incubated at 37°C with 5% CO₂ in a humidified incubator for 24 hr. BV2 cells were respectively treated with six different OPPs at gradient concentrations (0, 125, 250, 500, 1,000 μ M) for 24 hr. For the intervention group, BV2 cells were pre-treated with MCC950 (10 μ M) for 0.5 hr and then treated with OPPs for 24 hr.

2.3. Cell Viability Assay

To conduct the cell viability assay, the growth medium was removed from the BV2 cells cultured in a 96-well plate. The CCK-8 reagent was mixed with complete medium (1:9 volume ratio), and 100 μ L of the CCK-8 reagent mixture was added to each well. The plate was incubated for 4 hr, and absorbance was measured at 450 nm using a microplate reader (BNR05740; Molecular Devices, Sunnyvale, CA, USA). The average absorbance from each sextuplicate set of wells was calculated, and the background control value was subtracted from the absorbance value. The percentage of viable cells was determined using the following equation:

$$\text{Cell viability (\%)} = [(A_s - A_b) / (A_c - A_b)] \times 100,$$

where A_s is the absorbance of the experimental well (containing the medium, CCK-8 reagent, cells, and compound), A_c is the absorbance of the control well (containing the medium, CCK-8 reagent, and cells), and A_b is the absorbance of the blank well (containing the medium and CCK-8 reagent).

2.4. LDH-Based Cytotoxicity Assay

To use the Cytotoxicity LDH Assay Kit, lysis buffer (10 μ L) was added to the high control well of a 96-well plate containing BV2 cells, which was then incubated for 0.5 hr. The working solution was prepared by adding 5 mL of the assay buffer to the dye mixture vial, of which 100 μ L was added to each well. The plate was protected from light and incubated at room temperature for 0.5 hr. Subsequently, 50 μ L of stop solution was added to each well, and the absorbance was measured immediately at 490 nm using a microplate reader (BNR05740, Molecular Devices). The average absorbance was calculated from each sextuplicate set of wells, and the background control value was subtracted from the absorbance value. The percentage of cytotoxicity was determined using the following equation:

$$\text{Cytotoxicity (\%)} = [(A_a - A_{b1}) / (A_{b2} - A_{b1})] \times 100,$$

where A_a is the absorbance of the experimental well (containing medium, cells, and compound), A_{b2} is the absorbance of the high control well (containing medium, cells, and lysis buffer), and A_{b1} is the absorbance of the low control well (containing medium and cells).

2.5. Real-Time Quantitative PCR (RT-qPCR)

TRIzol Reagent (1 mL) was directly added to BV2 cells in 6-well plates, and total RNA was extracted according to the manufacturer's instructions. Total RNA was used for cDNA reverse transcription, which was performed according to the PrimeScript RT protocol with the following reaction conditions: 42°C for 2 min, 4°C for ∞ (removal of genomic DNA), 37°C for 15 min, 85°C for 5 s, and 4°C for ∞ (reverse transcriptional reaction). The RT-qPCR was performed in accordance with the TB Green Premix Ex Taq II protocol. Primer sequences and product lengths were as follows: NLRP3 (83 bp) forward primer 5'-ATTACCGCCCGAGAAAGG-3', reverse primer 5'-CATGAGTGTGGCTAGATCCAAG-3'; ASC (90 bp) forward primer 5'-GTGGACGGAG

TGCTGGAT-3', reverse primer 5'-CTTGTCTTGGCTGGTGGT-3'; Caspase-1 (121 bp) forward primer 5'-GGACATCCTTCATCCTCAGAAACA-3', reverse primer 5'-TTTCTTCCATAACTTCTGGGCTTT-3'; IL-1 β (76 bp) forward primer 5'-ACAGGCTCCGAGATGAACAAC-3', reverse primer 5'-CCATTGAGGTGGA-GAGCTTTC-3'; IL-18 (202 bp) forward primer 5'-GTGAACCCCAGACCAGACTG-3', reverse primer 5'-CCTGGAACACGTTTCTGAAAGA-3'; and β -actin (154 bp) forward primer 5'-GGCTGTATCCCCTC-CATCG-3', reverse primer 5'-CCAGTTGGTAACAATGCCATGT-3'. RT-qPCR was performed using the CFX96 Real-Time System (Bio-Rad Laboratories, Hercules, CA, USA) with the following reaction conditions: 95°C for 30 s, 40 cycles of 95°C for 5 s, 61°C for 30 s, and 72°C for 30 s, followed by a melting curve from 65 to 95°C in 0.5°C/5 s increments. Calculations were performed using the CFX Manager™ Version 1.0 software (Bio-Rad Laboratories Ltd., USA) and are represented as fold-change in expression [$2^{\Delta\Delta C(t)}$] on a linear scale.

2.6. Detection of Proinflammatory Cytokines

The ELISA kits (cat. ab197742 and ab216165) were used to quantify the IL-1 β and IL-18 secreted into the culture supernatants of BV2 cells after incubation for 24 hr, following the manufacturer's instructions. BV2 cell culture supernatants were centrifuged and collected at 2,000 rpm for 10 min to remove the remaining cells. Next, 50 μ L of the sample, standard, and antibody cocktails were added to each well. The plates were incubated for 1 hr at room temperature on a shaker at 400 rpm. Each well was washed with 350 μ L wash buffer, and 100 μ L of TMB solution was added to each well and incubated for 10 min in the dark on a shaker at 400 rpm. Then, 100 μ L of stop solution was added to each well. The absorbance was recorded at 450 nm using a microplate reader (BNR05740, Molecular Devices). For IL-1 β and IL-18 extracellular expression, standard curves were created from 1.56 to 100 pg/mL and 31.3 to 2,000 pg/mL, with sensitivities of 1 and 10.5 pg/mL, and concentrations were expressed as pg/mL, respectively.

2.7. Two-Stage Mass Spectrometry (MS/MS) Analysis

NLRP3 recombinant proteins were separated by sodium dodecyl-sulfate polyacrylamide gel electrophoresis (SDS-PAGE) and stained with Coomassie Brilliant blue (CBB) R-250; NLRP3 protein bands were precisely excised on a clean glass plate using a sharp blade. Peptides (2 μ L) were analyzed at high resolution using a NanoLC-Orbitrap Elite MS/MS system (Thermo Fisher Scientific, Co., Ltd. USA) with an automatic sampler for data acquisition. The system was operated in positive ion spray ionization mode, with an injection speed of 0.3 μ L/min, capillary voltage of 2.2 kV, mass-to-charge ratio range of 300–1,800 m/z, and 35% collision energy. Data were processed using Proteome Discovery 2.4. Qualitative assessment of proteins and mass-to-charge ratios (m/z) of fragment peaks were performed by comparing the differences in the MS/MS spectra.

2.8. Surface Plasmon Resonance (SPR) Analysis

The binding capacity of the hNLRP3 LRR recombinant protein to OPPs was determined by SPR according to the Biacore 8 K system (Cytiva, USA) using the CM5 chip. After obtaining the baseline signal, the sample loop was flushed with phosphate-buffered saline (PBS), and 80 μ g/mL of hNLRP3 protein (diluted by acetate as pH 4.0) was added and contacted for 10 min at 10 μ L/min and 25°C. The following analytes were used: paraoxon (15.625, 62.5, 125, 250, 500 μ M), dichlorvos (31.25, 62.5, 125, 250, 500 μ M), fenthion (62.5, 125, 250, 500, 1,000 μ M), dipterex (62.5, 125, 250, 500, 1,000 μ M), dibrom (7.8125, 62.5, 250, 500, 1,000 μ M), and dimethoate (31.25, 125, 250, 500, 1,000 μ M). The contact and dissociation times of the analytes and proteins were 120 and 300 s, respectively. An affinity model was used to determine the association (k_a), dissociation (k_d), and affinity constants (K_D).

2.9. Molecular Docking

The macromolecular structure of the hNLRP3 inflammasome used for molecular docking simulation was obtained from the Protein Data Bank (PDB ID 6NPY, <https://www.rcsb.org>), and undesired structures were managed using the SEQ module of the Molecular Operating Environment (MOE) version 20.09 software (Sharif et al., 2019; S. Wang et al., 2021; X. N. Wang et al., 2021; Yang et al., 2019). The structures of the OPPs (paraoxon, dichlorvos, fenthion, dipterex, dibrom, and dimethoate) were derived from the PubChem database (<https://pubchem.ncbi.nlm.nih.gov/>) in SDF format. Small molecules were minimized and saved. Macromolecular docking pockets were determined using the Site Finder module. Molecular docking simulations were

performed using the Docking Module, and all docking processes were completed under an Amber 10: EHT force field, using an R-field dominant solvent model with a pH of 7.0 and a temperature of 300 K. The generalized-Born volume integral/weighted surface area (GBVI/WSA) dG scoring function was used to score the 30 structures, with London dG scores for flexible docking (S. Wang et al., 2021; X. N. Wang et al., 2021; Yang et al., 2019). Macromolecules and small molecules have been screened for improved interaction performance.

2.10. Statistical Analysis

The experimental data are expressed as the standard error of the mean (SEM). GraphPad Prism version 6.0 software (GraphPad Software, La Jolla, CA, USA) was used for the data analysis. One-way analysis of variance for multiple comparisons was used to analyze differences between groups, and $P < 0.05$ was considered statistically significant.

3. Results

3.1. OPPs-Induced Cytotoxicity in BV2 Cells

3.1.1. OPPs Treatment Decreases the Cell Viability in BV2 Cells

To determine the cytotoxicity of six different OPPs compounds in BV2 cells, cell viability was evaluated using a CCK-8 kit after treatment with different kinds and concentrations of OPPs for 24 hr. Compared with treatment with 0 μM OPPs, the cell viability of BV2 cells treated with paraoxon (125 μM , $P < 0.01$; 250 μM , $P < 0.0001$; 500 μM , $P < 0.0001$; 1,000 μM , $P < 0.0001$) (Figure S1a in Supporting Information S1), dichlorvos (125 μM , $P < 0.01$; 250 μM , $P < 0.0001$; 500 μM , $P < 0.0001$; 1,000 μM , $P < 0.0001$) (Figure S1b in Supporting Information S1), fenthion (500 μM , $P < 0.001$; 1,000 μM , $P < 0.0001$) (Figure S1c in Supporting Information S1), dipterex (125 μM , $P < 0.05$; 250 μM , $P < 0.01$; 500 μM , $P < 0.0001$; 1,000 μM , $P < 0.0001$) (Figure S1d in Supporting Information S1), dibrom (250 μM , $P < 0.05$; 500 μM , $P < 0.0001$; 1,000 μM , $P < 0.0001$) (Figure S1e in Supporting Information S1), and dimethoate (125 μM , $P < 0.001$; 250 μM , $P < 0.001$; 500 μM , $P < 0.01$; 1,000 μM , $P < 0.01$) (Figure S1f in Supporting Information S1) significantly decreased.

3.1.2. OPPs Increased the Cytotoxicity in BV2 Cells

The cytotoxic effects of OPPs in BV2 cells were further detected using the LDH assay after treatment with different kinds and concentrations of OPPs for 24 hr. Compared with treatment with 0 μM OPPs, BV2 cells treated with paraoxon (125 μM , $P < 0.001$; 250 μM , $P < 0.0001$; 500 μM , $P < 0.0001$; 1,000 μM , $P < 0.0001$) (Figure S2a in Supporting Information S1), dichlorvos (125 μM , $P < 0.0001$; 250 μM , $P < 0.001$; 500 μM , $P < 0.0001$; 1,000 μM , $P < 0.0001$) (Figure S2b in Supporting Information S1), fenthion (250 μM , $P < 0.01$; 500 μM , $P < 0.01$; 1,000 μM , $P < 0.001$) (Figure S2c in Supporting Information S1), dipterex (125 μM , $P < 0.01$; 250 μM , $P < 0.0001$; 500 μM , $P < 0.001$; 1,000 μM , $P < 0.0001$) (Figure S2d in Supporting Information S1), dibrom (125 μM , $P < 0.001$; 250 μM , $P < 0.0001$; 500 μM , $P < 0.0001$; 1,000 μM , $P < 0.0001$) (Figure S2e in Supporting Information S1), and dimethoate ($P < 0.0001$) (Figure S2f in Supporting Information S1) significantly increased cytotoxicity. These findings indicate that all six types of OPPs demonstrated obvious cytotoxic effects on BV2 cells.

Furthermore, the cytotoxic effect based on half effective inhibition concentration (IC_{50}) values of OPPs in BV2 cells were listed in the following order: dichlorvos > dipterex > paraoxon > dibrom > fenthion > dimethoate, and the corresponding IC_{50} values as 274, 410, 551, 585, 2,158, and 1,527,566 μM (Table 1). All six OPPs showed pronounced cytotoxic effects on BV2 cells, among which dichlorvos demonstrated the strongest cytotoxicity.

3.2. OPPs Activate NLRP3 Inflammasome and Increase Inflammatory Cytokines in BV2 Cells

Our research revealed an obvious cytotoxic effect of OPPs on BV2 cells. However, the mechanism underlying OPPs poisoning has not yet been fully elucidated. Previous studies have shown that the NLRP3 inflammasome can be activated by cholesterol, trimethyltin, acrylamide, sevoflurane, and other compounds with electrophilic organic characteristics, resulting in a series of inflammatory or abnormal physiological reactions (Duell et al., 2010; Long et al., 2019; Sharif et al., 2019; Sui et al., 2020). Therefore, we hypothesized that the NLRP3 inflammasome may be a common target of several different OPPs. The results showed that the expression of NLRP3, ASC, Caspase-1, IL-1 β , IL-18, and mRNA in BV2 cells treated with 500 μM paraoxon, dichlorvos,

Table 1
IC₅₀ Values of OPPs in BV2 Cells

Toxicants	BV2 cells (μM)	BV2 cells + MCC950 (10 μM) (μM)
Paraoxon	551	1,282
Dichlorvos	274	358
Fenthion	2,158	3,304
Dipterex	410	492
Dibrom	585	762
Dimethoate	1,527,566	2,666,859

fenthion, dipterex, dibrom, and dimethoate were significantly increased, respectively (compared with that in 0 μM OPPs-treated cells, $P < 0.0001$, Figures S3a–S3e in Supporting Information S1). Thus, the six OPPs significantly increased the expression of NLRP3 inflammasome complexes and downstream inflammatory cytokines in BV2 cells.

3.3. MCC950 Reverses the Expression of NLRP3 Inflammasome Complexes and Inflammatory Cytokines Induced by OPPs in BV2 Cells

Changes in OPPs-induced cytotoxicity were measured after blocking the NLRP3 inflammasome to determine whether it was a crucial target involved in OPPs poisoning. Compared with the OPPs treatment group (500 μM), those pre-treated with MCC950 (10 μM, NLRP3 inflammasome specific inhibitor) exhibited a significant decrease in NLRP3 mRNA expression in BV2 cells treated with paraoxon ($P < 0.05$), dichlorvos ($P < 0.0001$), fenthion ($P < 0.0001$), dipterex ($P < 0.0001$), dibrom ($P < 0.0001$), and dimethoate ($P < 0.0001$) (Figure 1a). ASC mRNA expression in BV2 cells treated with paraoxon ($P < 0.0001$), dichlorvos ($P < 0.0001$), fenthion ($P < 0.0001$), dipterex ($P < 0.01$), dibrom ($P < 0.001$), and dimethoate ($P < 0.0001$) also decreased after MCC950 intervention (Figure 1b). Otherwise, Caspase-1 and IL-18 mRNA expressions in BV2

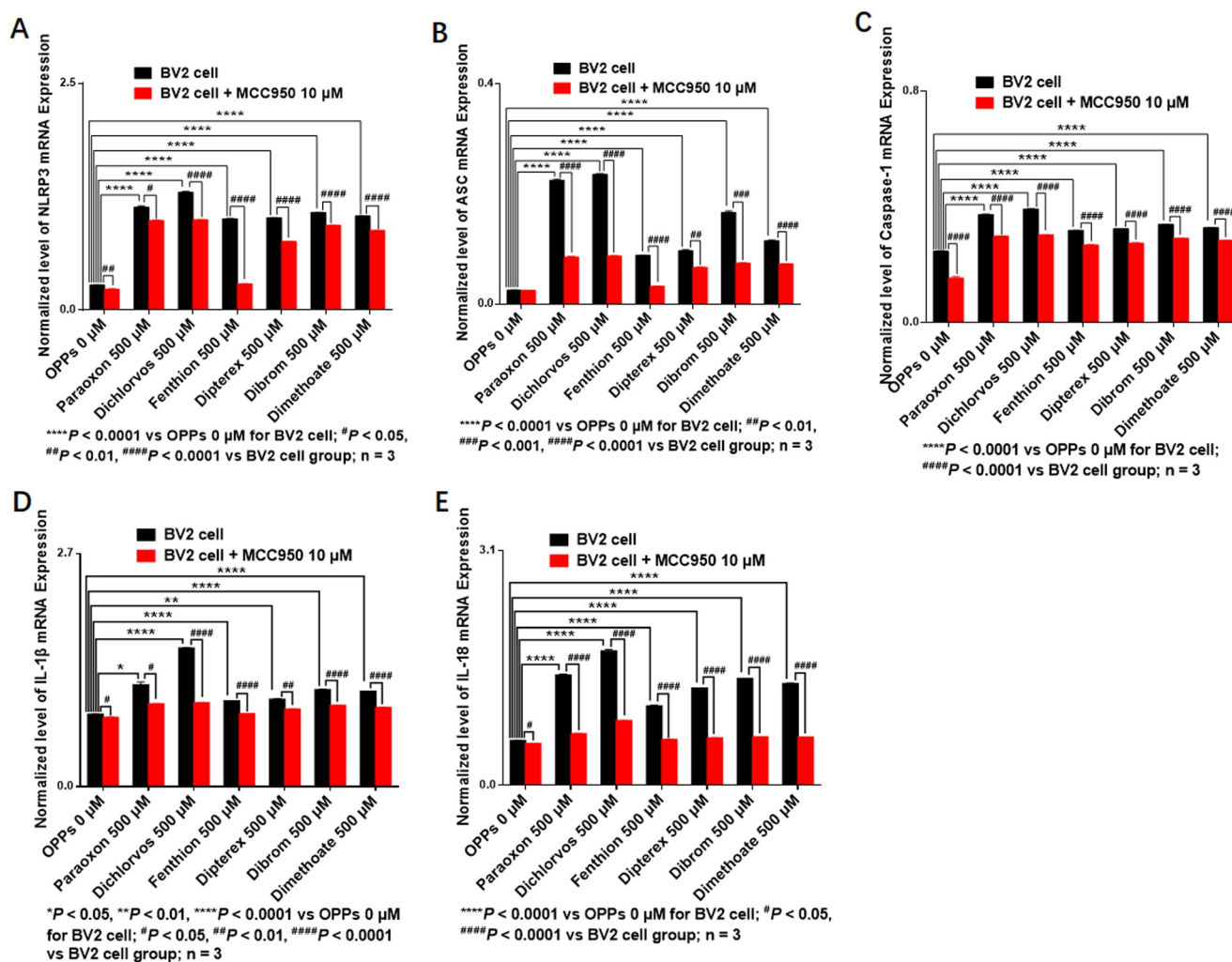


Figure 1. mRNA expression changes of the NLRP3 inflammasome and associated inflammatory cytokines in BV2 cells treated with OPPs and MCC950 intervention. (a) mRNA Expression of NLRP3, (b) mRNA Expression of ASC, (c) mRNA Expression of Caspase-1, (d) mRNA Expression of IL-1β, and (e) mRNA Expression of IL-18.

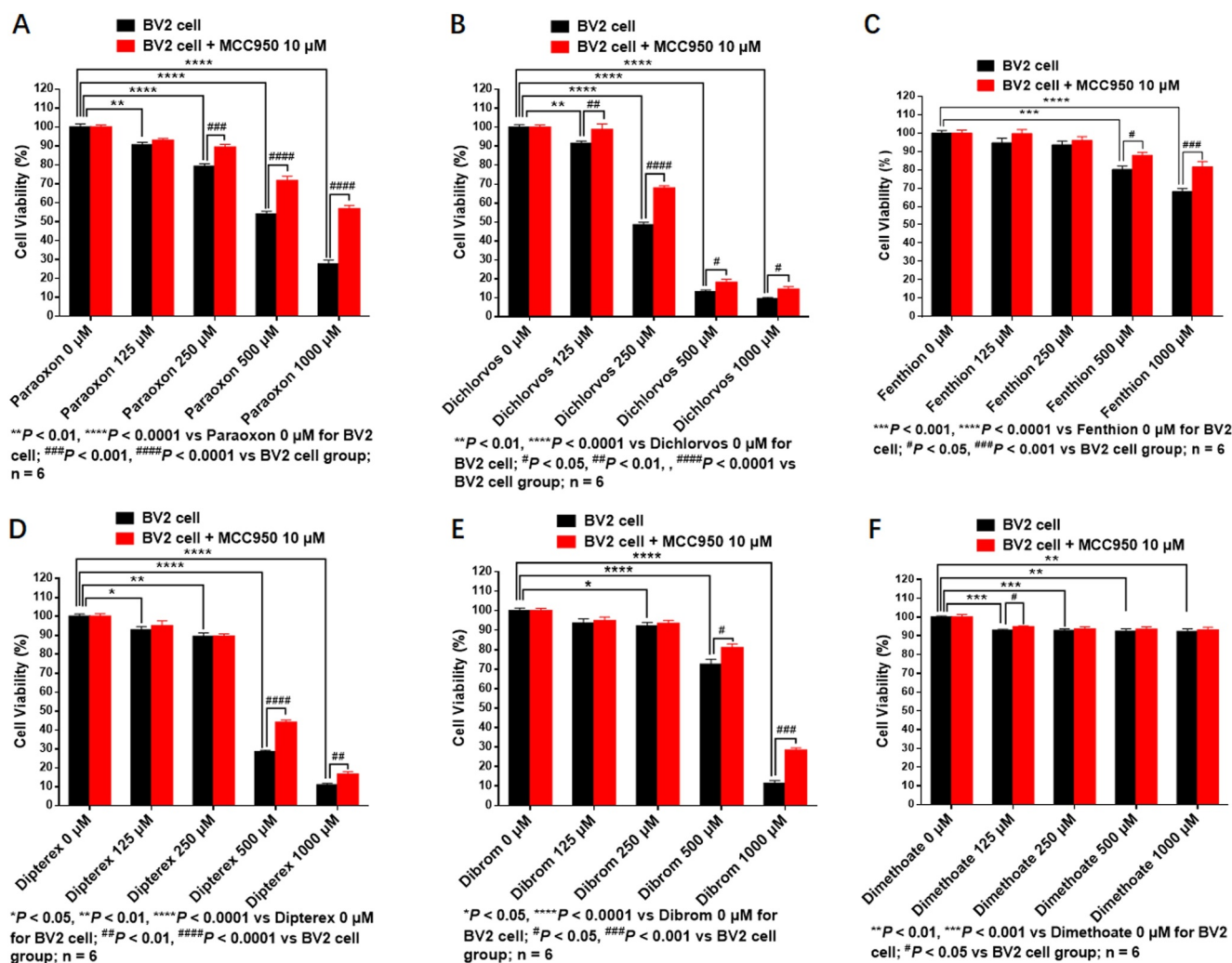


Figure 2. Cell viability of BV2 cells treated with OPPs and MCC950 intervention. BV2 cells treated with different concentrations of (a) paraoxon, (b) dichlorvos, (c) fenthion, (d) dipterex, (e) dibrom, and (f) dimethoate.

cells treated with paraoxon, dichlorvos, fenthion, dipterex, dibrom, and dimethoate were significantly decreased, respectively (Figures 1c and 1e, $P < 0.0001$), and IL-1 β mRNA expression after treatment with paraoxon ($P < 0.05$), dichlorvos ($P < 0.0001$), fenthion ($P < 0.0001$), dipterex ($P < 0.01$), dibrom ($P < 0.0001$), and dimethoate ($P < 0.0001$) (Figure 1d) was decreased by MCC950 intervention, respectively. These results indicated that MCC950 intervention reduced the activation of the NLRP3 inflammasome and associated inflammatory cytokine mRNA expression in multiple OPPs-treated BV2 cells.

3.4. MCC950 Reduced the Cytotoxicity of BV2 Cells Induced by OPPs

3.4.1. MCC950 Increased the Cell Viability of BV2 Cells Induced by OPPs

Compared with those following OPPs treatment (125, 250, 500, 1,000 μM), BV2 cells pre-treated with inflammasome specific inhibitor MCC950 (10 μM) significantly increased cell viability of BV2 cells treated with paraoxon (250 μM , $P < 0.001$; 500 μM , $P < 0.0001$; 1,000 μM , $P < 0.0001$) (Figure 2a), dichlorvos (125 μM , $P < 0.01$; 250 μM , $P < 0.0001$; 500 μM , $P < 0.05$; 1,000 μM , $P < 0.05$) (Figure 2b), fenthion (500 μM , $P < 0.05$; 1,000 μM , $P < 0.001$) (Figure 2c), dipterex (500 μM , $P < 0.0001$; 1,000 μM , $P < 0.01$) (Figure 2d), dibrom (500 μM , $P < 0.05$; 1,000 μM , $P < 0.001$) (Figure 2e), and dimethoate (125 μM , $P < 0.05$) (Figure 2f). These results indicated that NLRP3 may play a critical role in OPPs-induced cytotoxicity.

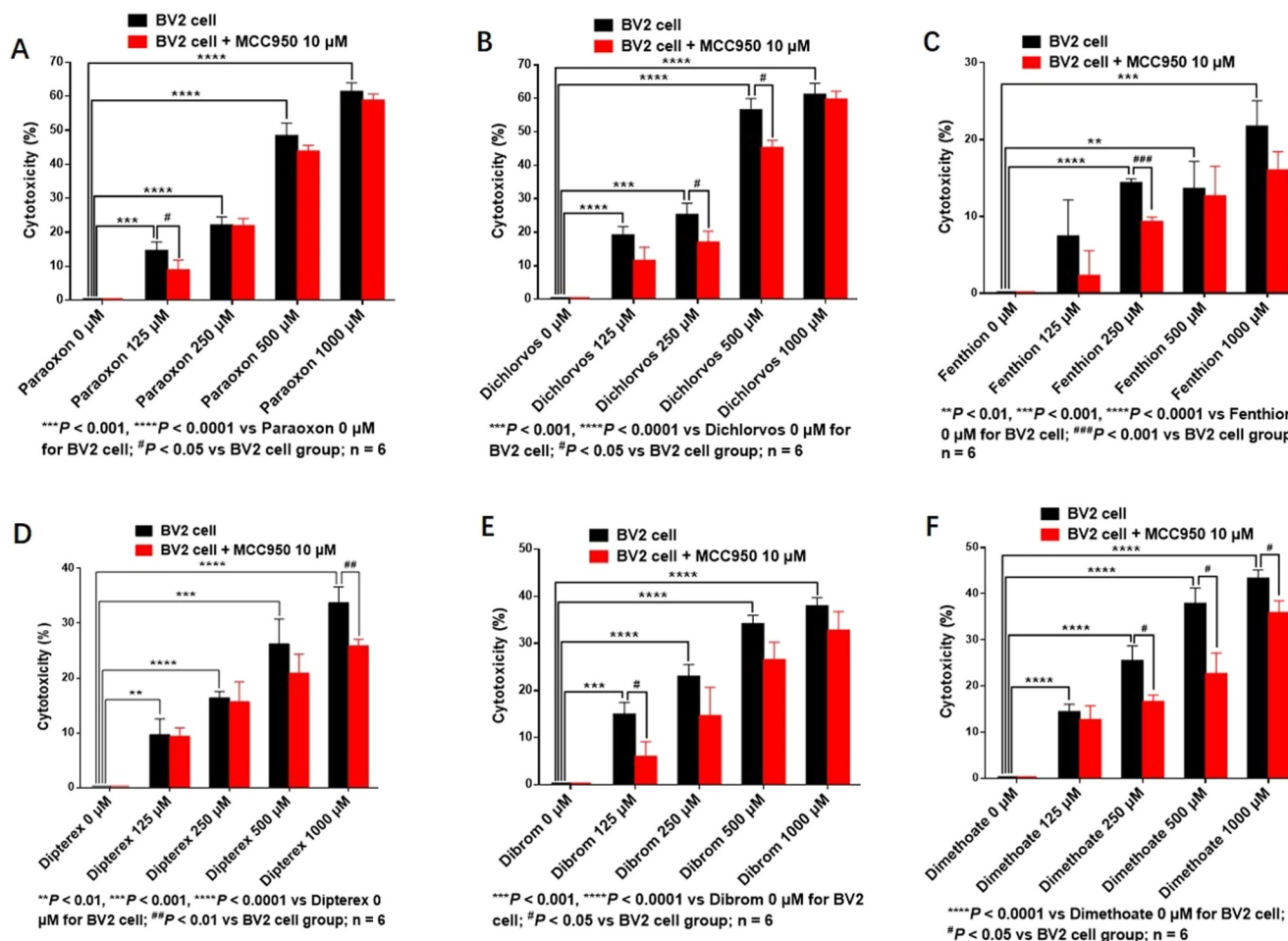


Figure 3. Cytotoxicity of BV2 cells treated with OPPs were decreased by MCC950 intervention. (a) Paraoxon, (b) dichlorvos, (c) fenthion, (d) dipterex, (e) dibrom, and (f) dimethoate.

3.4.2. MCC950 Decreased the Cytotoxicity of BV2 Cells Induced by OPPs

Compared with OPPs treatment (125, 250, 500, 1,000 μM), BV2 cells pre-treated with MCC950 (10 μM) exhibited significantly decreased cytotoxicity when treated with paraoxon (125 μM, $P < 0.05$) (Figure 3a), dichlorvos (250 μM, $P < 0.05$; 500 μM, $P < 0.05$) (Figure 3b), fenthion (250 μM, $P < 0.001$) (Figure 3c), dipterex (1,000 μM, $P < 0.01$) (Figure 3d), dibrom (125 μM, $P < 0.05$) (Figure 3e), and dimethoate (250 μM, $P < 0.05$; 500 μM, $P < 0.05$; 1,000 μM, $P < 0.05$) (Figure 3f). Moreover, the IC_{50} values of BV2 cells treated with paraoxon, dichlorvos, fenthion, dipterex, dibrom, and dimethoate after MCC950 (10 μM) intervention were 1,282, 358, 3,304, 492, 762, and 2,666,859 μM, respectively (Table 1), which indicated that MCC950 could markedly decrease cytotoxicity induced by OPPs.

3.5. MCC950 Decreased the IL-1β and IL-18 mRNA Expression in an Extracellular Medium of BV2 Cells Treated With OPPs

These results indicated that NLRP3 is a potential key target for OPPs-induced BV2 cell cytotoxicity. The NLRP3 inflammasome is a large molecular platform activated by various chemicals that trigger cellular cascade responses after activating inflammatory caspases and processing pro-IL-1β and pro-IL-18 (Kelly et al., 2019; Man & Kanneganti, 2015; Takahashi, 2019). IL-1β and IL-18 expression in the extracellular medium of BV2 microglia were determined by ELISA assay after treatment with OPPs (125, 250, 500 μM) for 24 hr. Compared with treatment with 0 μM OPPs, the expression of IL-1β and IL-18 in the extracellular medium of BV2 cells treated with paraoxon, dichlorvos, fenthion, dipterex, dibrom, and dimethoate were all significantly increased

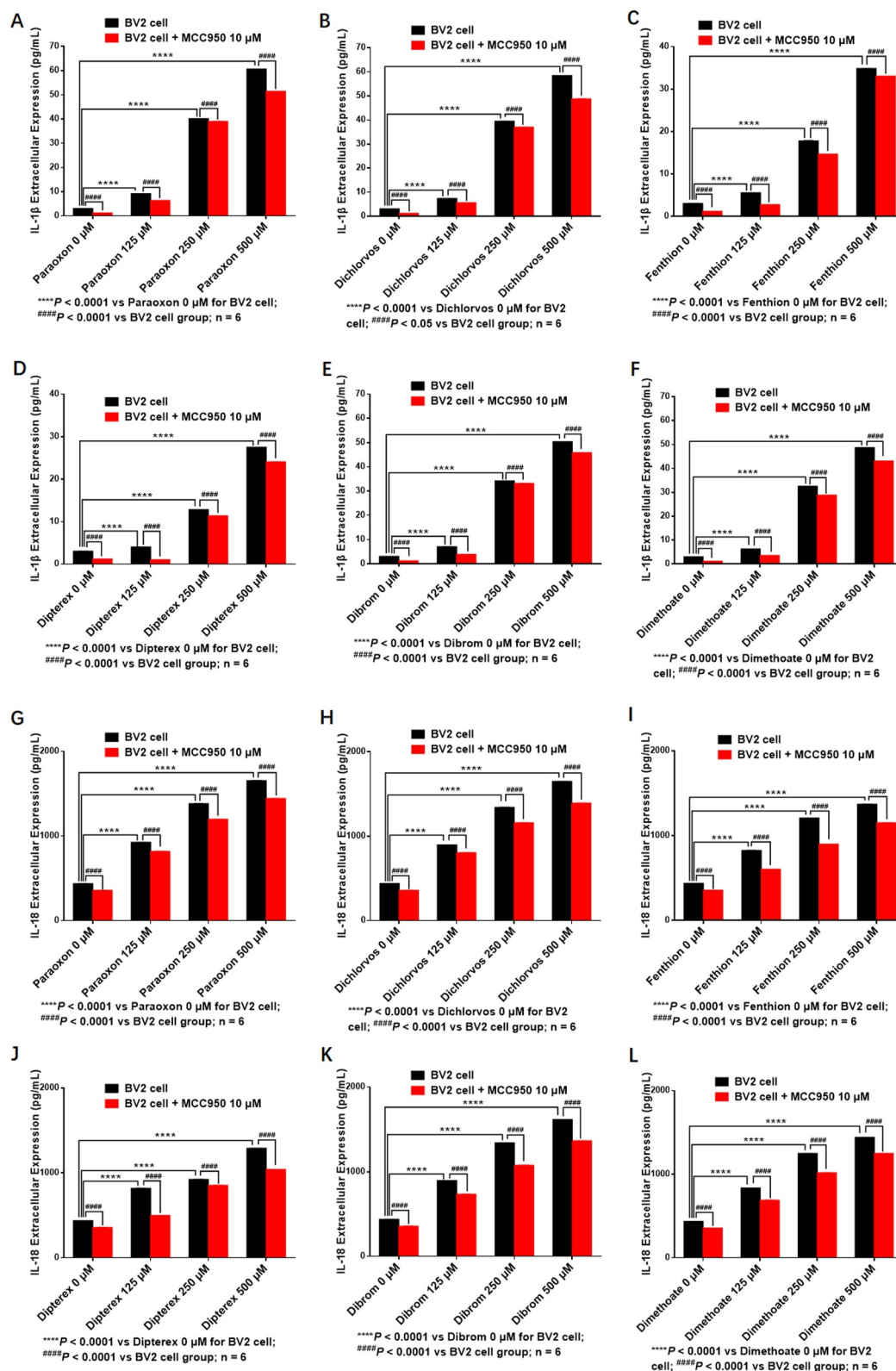


Figure 4. IL-1 β and IL-18 extracellular expressions in BV2 cells treated with OPPs were decreased by MCC950 intervention. (a) Paraoxon, (b) dichlorvos, (c) fenthion, (d) Dipterex, (e) dibrom, (f) dimethoate for IL-1 β expression; (g) paraoxon, (h) dichlorvos, (i) fenthion, (j) dipterex, (k) dibrom, and (l) dimethoate for IL-18 expression.

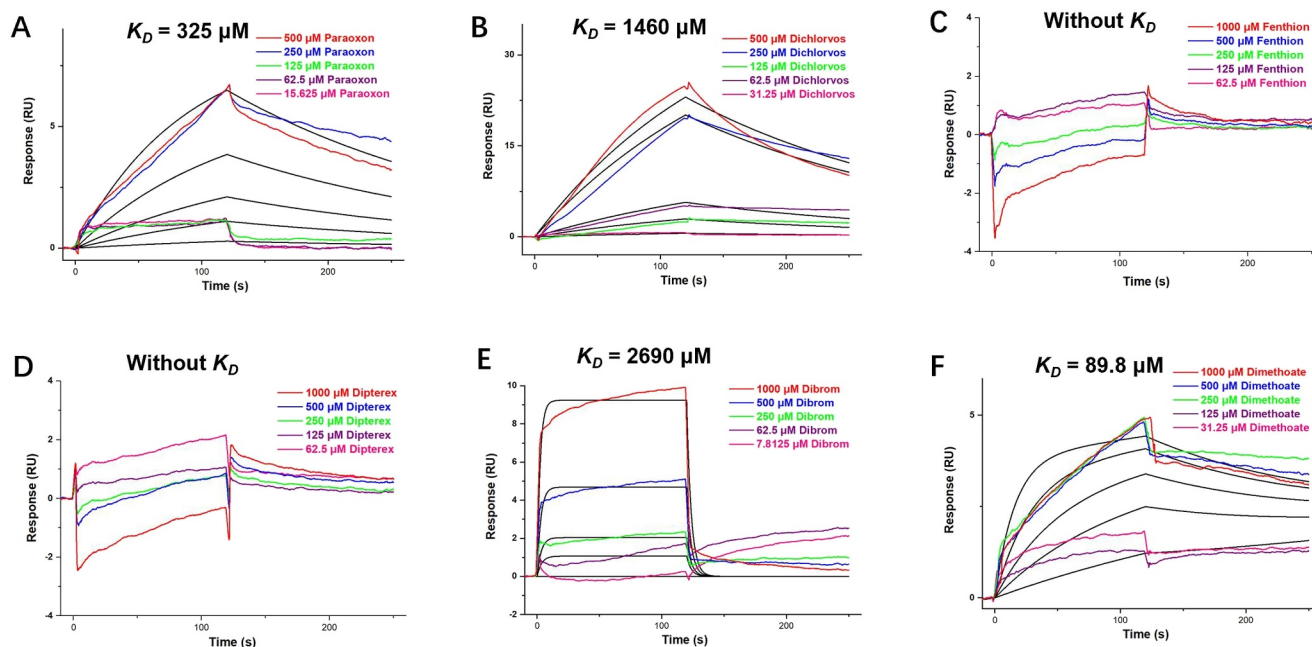


Figure 5. Affinity curves and constants of hNLRP3 and OPPs. (a) Paraoxon, (b) dichlorvos, (c) fenthion, (d) dipterex, (e) dibrom, and (f) dimethoate. K_D : affinity constant.

(Figures 4a–4l, $P < 0.0001$). Compared with OPPs treatment (125, 250, 500 μM), MCC950 (10 μM) intervention exhibited significantly reduced IL-1 β and IL-18 expression in the extracellular medium of BV2 cells, respectively (Figures 4a–4l, $P < 0.0001$). In summary, the expression of IL-1 β and IL-18 in OPPs-induced BV2 cells was significantly decreased by MCC950 treatment. NLRP3 is an essential target that mediates downstream cytokine expression and contributes to OPPs toxicity in BV2 cells.

3.6. Molecular Mechanism of the NLRP3-OPPs Interaction

3.6.1. Tandem Mass Spectrometry (MS/MS) Results

The amino acid sequence of the hNLRP3 LRR protein was confirmed using MS/MS. The SDS-PAGE analysis indicated that the molecular weight of the hNLRP3 LRR was 41 kDa (Figure S4a in Supporting Information S1). The secondary structure was determined by collision-induced dissociation (CID), and m/z was determined by MS/MS after enzymology (Figures S4c–S4m and Table S1 in Supporting Information S1) and indicated that the molecular weight and amino acid sequence of the purchased hNLRP3 LRR were consistent with the corresponding sequences on the National Center for Biotechnology Information (NCBI) website (Figure S4b in Supporting Information S1).

3.6.2. Affinity of hNLRP3 for OPPs

SPR analysis indicated that k_a , k_d , and K_D values of hNLRP3-paraoxon were $14.2 \text{ M}^{-1} \text{ s}^{-1}$, 0.00461 s^{-1} , and $325 \text{ }\mu\text{M}$, respectively (Figure 5a). Those for hNLRP3-dichlorvos were $3.35 \text{ M}^{-1} \text{ s}^{-1}$, 0.00489 s^{-1} , and $1,460 \text{ }\mu\text{M}$, respectively (Figure 5b). Those for hNLRP3-dibrom were $76.5 \text{ M}^{-1} \text{ s}^{-1}$, 0.206 s^{-1} , and $2,690 \text{ }\mu\text{M}$, respectively (Figure 5e). Those for hNLRP3-dimethoate were $58.9 \text{ M}^{-1} \text{ s}^{-1}$, 0.00529 s^{-1} , and $89.8 \text{ }\mu\text{M}$, respectively (Figure 5f). No obvious binding was detected between hNLRP3 and fenthion or dipterex at the concentrations mentioned above (Figures 5c and 5d). The order of k_a values for OPPs-hNLRP3 was dibrom > dimethoate > paraoxon > dichlorvos > (fenthion and dipterex). The order of the k_d values for OPPs-hNLRP3 was paraoxon > dichlorvos > dimethoate > dibrom > (fenthion and dipterex). The order of K_D values for OPPs-hNLRP3 was dimethoate > paraoxon > dichlorvos > dibrom > (fenthion and dipterex). In summary, paraoxon, dichlorvos, dibrom, and dimethoate showed stronger bindings to hNLRP3, whereas no obvious affinity was observed between hNLRP3 and fenthion or dipterex.

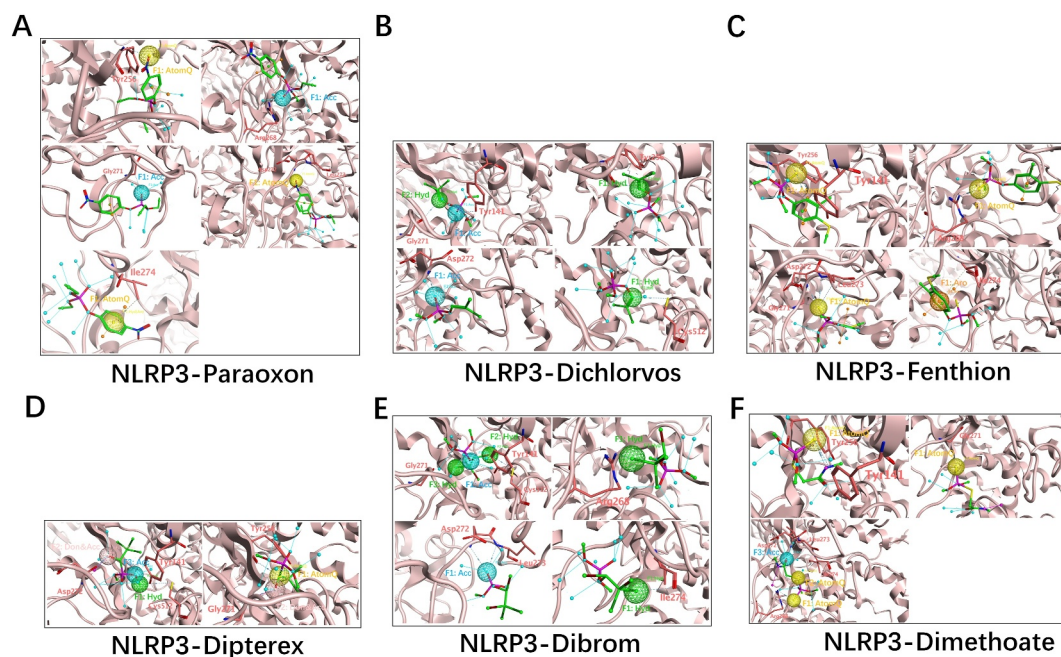


Figure 6. Interactions between NLRP3 and OPPs determined by molecular docking simulations. (a) Paraoxon, (b) dichlorvos, (c) fenthion, (d) dipterex, (e) dibrom, and (f) dimethoate.

3.6.3. Common Mechanism of hNLRP3-OPPs Interactions

The common mechanism of interaction between hNLRP3 and OPPs was clarified in detail using computational docking simulations. The OPPs contain hydrophobic (benzene ring and hydrocarbon chain) and active ($-O-$, $=O$, $-S-$, $=S$, $-Cl$, and $-Br$) groups (Figures S5a, S5b, S5d, S5e, S5g, S5h, S5j, S5k, S5n, S5p, and S5q in Supporting Information S1). The main structural differences between OPPs include side chain groups, hydrocarbon chains, and halogen content. Existing interaction residues of NLRP3-OPPs were obtained as follows: NLRP3-paraoxon, including Phe255, Tyr256, Arg268, Gly271, Asp272, Leu273, Ile274, and Lys514. NLRP3-dichlorvos, including Tyr141, Leu254, Tyr256, Gly271, Asp272, and Cys512. NLRP3-fenthion, including Tyr141, Tyr256, Glu261, Arg268, Gly271, Asp272, Leu273, and Ile274. NLRP3-dipterex, including Lys137, Tyr141, Tyr256, Ile257, His258, Leu270, Gly271, Asp272, Met275, Cys278, Cys512, and Glu513. NLRP3-dibrom, including Tyr141, Leu254, Arg268, Ser269, Gly271, Asp272, Leu273, Ile274, Cys277, and Cys512. NLRP3-dimethoate, including Tyr141, Tyr256, Arg268, Ser269, Gly271, Asp272, Leu273, Ile274, Ser276, Asn282, and Ala323. The key toxicity-effector groups of OPPs combined with NLRP3 were as follows: key groups of paraoxon, including the benzene ring, hydrocarbon chain, $-O-$, and $=O$, and toxic-effecting groups, including Acc, Aro, Hyd, and AtomQ (Figure S5c in Supporting Information S1); dichlorvos, including the hydrocarbon chain, $-(C=CH-)$, $=O$, Acc, and Hyd (Figure S5f in Supporting Information S1); fenthion, including the benzene ring, hydrocarbon chain, $=S$, Aro, and AtomQ (Figure S5i in Supporting Information S1); dipterex, including hydrocarbon chains, $-(CH-)$, $-O-$, Acc, Don, Hyd, and AtomQ (Figure S5l in Supporting Information S1); dibrom, including hydrocarbon chains, $-Cl$, $-Br$, $-O-$, $=O$, Acc, and Hyd (Figure S5o in Supporting Information S1); and dimethoate, including hydrocarbon chains, $=O$, $-S-$, $=S$, Acc, and AtomQ (Figure S5r in Supporting Information S1).

The Cryo-EM structures of the NLRP3 inflammasome and the residues with high frequency (≥ 3) participating in NLRP3-OPPs were Tyr141, Tyr256, Arg268, Gly271, Asp272, Leu273, Ile274, and Cys512 (Figures S6a and S6b in Supporting Information S1). Therefore, residues with high frequency of NLRP3-paraoxon, including Tyr256, Arg268, Gly271, Asp272, Leu273, and Ile274 (Figure 6a, Figures S6c, S7d, and Table S2 in Supporting Information S1). NLRP3-dichlorvos, including Tyr141, Tyr256, Gly271, Asp272, and Cys512 (Figure 6b, Figures S6d, S7e, and Table S2 in Supporting Information S1). NLRP3-fenthion, including Tyr141, Tyr256, Arg268, Gly271, Asp272, Leu273, and Ile274 (Figure 6c, Figures S6e, S7f, and Table S2 in Supporting Information S1). NLRP3-dipterex, including Tyr141, Tyr256, Gly271, Asp272, and Cys512 (Figure 6d, Figures S6f,

S7g, and Table S2 in Supporting Information S1). NLRP3-dibrom, including Tyr141, Arg268, Gly271, Asp272, Leu273, Ile274, and Cys512 (Figure 6e, Figures S6g, S7h, and Table S2 in Supporting Information S1). NLRP3-dimethoate, including Tyr141, Tyr256, Arg268, Gly271, Asp272, Leu273, and Ile274 (Figure 6f, Figures S6h, S7i, and Table S2 in Supporting Information S1).

Key NLRP3-OPPs combination processes include hydrophobic interactions and hydrogen bonding. Key NLRP3-paraoxon combinations were hydrophobic interactions of π -H with Ile274 and hydrogen bonding with Tyr256 (64.1%), Arg268 (28.9%), Gly271 (34.2%), Asp272 (33.2%), and Leu273 (34.8%). NLRP3-dichlorvos of hydrogen bonding with Tyr141 (33.1%), Tyr256 (56.8%), Gly271 (38.9%), Asp272 (56.8%), and Cys512 (65.2%). NLRP3-fenthion of π -H with Ile274 and hydrogen bonding with Tyr141 (22.8%), Tyr256 (32.9%), Arg268 (22.9%), Gly271 (55.2%), Asp272 (66.2%), and Leu273 (32.2%). NLRP3-dipterex, including Tyr141 (63.2%), Tyr256 (33.8%), Gly271 (55.6%), Asp272 (22.9%), and Cys512 (53.1%). NLRP3-dibrom, including Tyr141 (33.8%), Arg268 (33.9%), Gly271 (53.1%), Asp272 (28.1%), Leu273 (36.2%), Ile274 (63.8%), and Cys512 (53.2%). NLRP3-dimethoate, including Tyr141 (22.8%), Tyr256 (65.3%), Arg268 (33.2%), Gly271 (35.2%), Asp272 (66.3%), Leu273 (29.8%), and Ile274 (36.1%). The sums of hydrogen bond scores were 195.2%, 250.8%, 232.2%, 228.6%, 302.1%, and 288.7% (Figure S7a and Table S2 in Supporting Information S1). Combination areas were 262.89, 222.24, 269.77, 222.87, 227.36, and 228.15 Å² (Figure S7b and Table S2 in Supporting Information S1). Binding energies were -2.65, -2.95, -2.64, -2.78, -2.04, and -2.89 kcal/mol, respectively (Table S2 in Supporting Information S1). OPPs-Tyr141 of NLRP3 has five hydrogen bonds, -Tyr256 has five, -Arg268 has four, -Gly271 has six, -Asp272 has six, -Leu273 has four, -Ile274 has two, -Cys512 has three, and OPPs-Ile274 has two. The order of hydrogen bonding between OPPs and NLRP3 from strongest to weakest was as follows: dibrom > dimethoate > dichlorvos > fenthion > dipterex > paraoxon (Figure S7a in Supporting Information S1). Combination areas were as follows: fenthion > paraoxon > dimethoate > dibrom > dipterex > dichlorvos (Figure S7b in Supporting Information S1). Binding energies (BEs) were as follows: dichlorvos > dimethoate > dipterex > paraoxon > fenthion > dibrom (Table S2 in Supporting Information S1). This research demonstrated that molecular weight (MW) of OPPs was inversely proportional to the absolute value of binding energy (IBE) by MW and IBE as abscissa and ordinate (Figure S7c in Supporting Information S1). A smaller MW and larger IBE represented a stronger NLRP3-OPPs interaction.

4. Discussion

Organophosphate pesticides, are known to be neurotoxic and can cause a range of adverse health effects in humans and animals, including inflammation and damage to the neurological system. Research suggests that exposure to OPPs can lead to an inflammatory response in the brain, which can contribute to secondary brain injury. This can manifest as cognitive deficits, memory impairment, and even neurodegenerative diseases. Specific antitoxic drugs for OPPs poisoning are currently limited, it is important to identify common mechanisms of toxicity and explore the development of specific therapeutic drugs (Fernandes et al., 2017; Martín et al., 2017). The study provides an innovative approach to developing treatments for inflammation caused by organophosphate poisoning by identifying the NLRP3 inflammasome as a potential therapeutic target. It also offers new insights into improving countermeasure drugs for inflammatory pathology and understanding the underlying mechanisms of MTMC.

OPPs can inhibit the activity of the enzyme acetylcholinesterase, resulting in an excessive accumulation of acetylcholine. Those can lead to serious dysfunction of both the central and peripheral nervous systems and eventually result in brain injury. While anticholinergic drugs and cholinesterase reactivators can effectively treat OPPs poisoning, they are not effective against non-cholinergic system-mediated injury mechanisms, such as inflammation. In addition to the cholinergic system dysfunction caused by OPPs, other toxic effects, such as endocrine disorders or immunotoxicity have been reported in male Sprague-Dawley rats poisoned with dimethylparaoxon and diethylparaoxon at a subcutaneous dose corresponding to 50% of the median lethal dose (Houzé et al., 2019). In addition, chlorpyrifos exerts a significant toxic effect on BV2 cells characterized by atrophic synapses, cell aggregation, inflammation, and autophagy (C. Zhang et al., 2019). This research evaluated the cytotoxicity of six different kinds of OPPs on BV2 microglia cells in vitro for the first time. The order of the cytotoxic effects of OPPs on BV2 cells was as follows: dichlorvos > dipterex > dibrom > paraoxon > fenthion > dimethoate. The results showed that OPPs had a pronounced toxic effect on BV2 cells, with dichlorvos getting the strongest effect. However, the precise toxic target for the inflammatory reactions induced by OPPs requires further study.

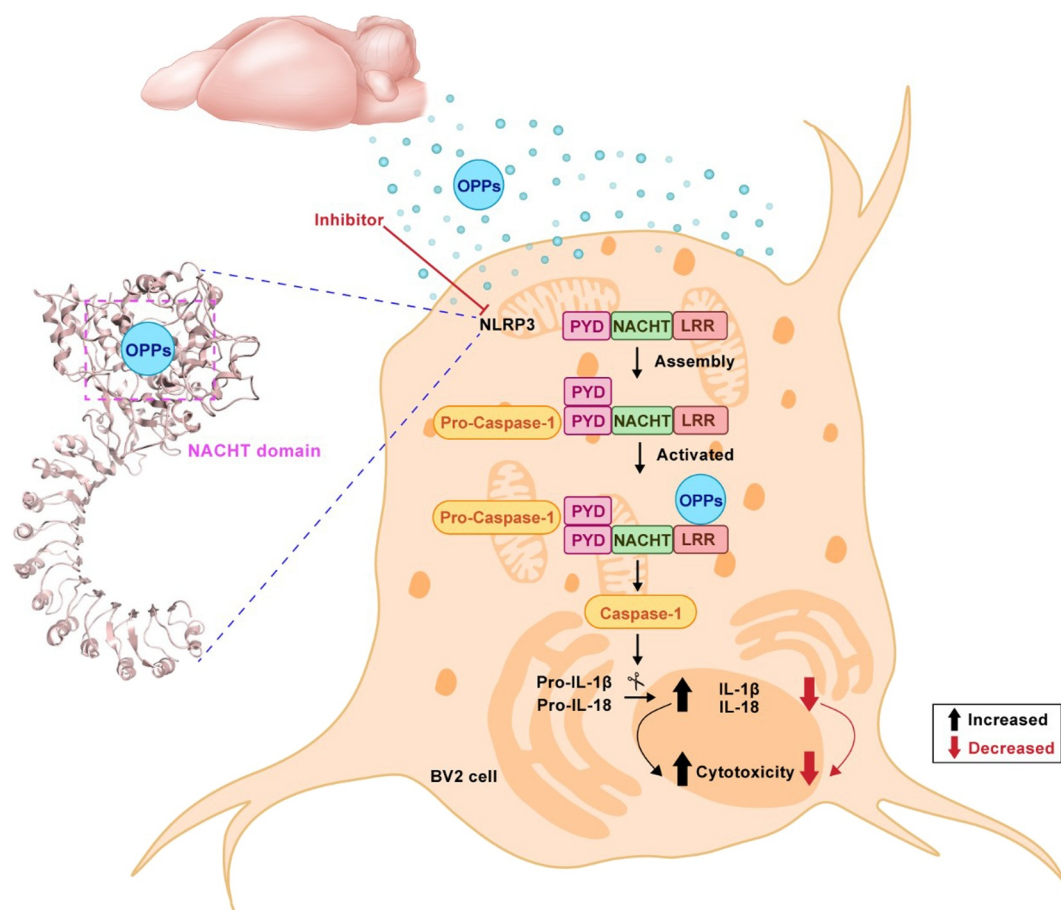


Figure 7. Potential cytotoxic mechanism in BV2 cells via NLRP3 inflammasome activation by OPPs-poisoning.

BV2 microglial cells, which are mononuclear phagocytes of the CNS, are important for the maintenance of CNS homeostasis and critically contribute to CNS pathology. Here, we demonstrated that the OPPs-regulatory NLRP3 inflammasome is crucial for regulating microglial activation and neuroinflammation during NLRP3/Caspase-1/ASC-dependent mechanisms (with IL-1 β and IL-18 release) (Lamkanfi & Dixit, 2014; Voet et al., 2018). Inflammasomes are cytoplasmic supermolecule complexes that form in response to exogenous microbial invasions and endogenous damage signals and are currently intensively discussed in the cytotoxicity community (Lamkanfi & Dixit, 2014; Zhu et al., 2023). NLRP3 inflammasome release Caspase-1 by OPPs, which process proinflammatory cytokines IL-1 β and IL-18 for maturation and cleave gasdermin to generate N-terminal fragments and induce pore formation, cytokines release, cell pyroptosis, and CNS injury (Kelly et al., 2019; X. Liu et al., 2016; Martín et al., 2017; S. Wang et al., 2021; X. N. Wang et al., 2021). The cytotoxic effects of OPPs treatment are complicated, and we will explore the relevant oxidative stress injuries and inflammatory reactions of BV2 cells treated with OPPs via the NLRP3 inflammasome or other receptors in the future. MCC950, a potent and selective inhibitor of the NLRP3 inflammasome, could specifically inhibit activation of the NLRP3 inflammasome at nanomolar concentrations, reducing ASC, Caspase-1, IL-1 β , and IL-18 intracellular or extracellular expressions, attenuating the severities of autoinflammatory and autoimmune diseases, and serving as a tool for further study of the NLRP3 inflammasome (Coll et al., 2015; Dempsey et al., 2017; Eychenne et al., 2022; Martín et al., 2017). In the present study, OPPs significantly increased mRNA expression of NLRP3 and associated inflammatory cytokines (ASC, Caspase-1, IL-1 β , IL-18), which could be decreased in BV2 cells by MCC950 intervention. It simultaneously demonstrated that NLRP3 was an essential target of the mediated expressions of IL-1 β and IL-18 in extracellular space, which was instrumental in the toxicity of OPPs toward BV2 cells (Figure 7). As shown in Figure 7, mechanism of BV2 cell injury caused by OPPs poisoning mediated by NLRP3 inflammasome was analyzed in this study. It was concluded that with increasing concentration of OPPs, cell viability decreased, damage increased, and expression of NLRP3 inflammasome and inflammatory factors IL-1 β /

-18 increased. BV2 was target cell for OPPs poisoning, and NLRP3 inflammasome was target protein of OPPs. Inhibition of NLRP3 inflammasome resulted in increased cell viability, decreased damage, and decreased expression of NLRP3 inflammasome and related inflammatory factors, indicating that OPPs caused BV2 cell damage based on NLRP3 inflammasome. These results suggested that the NLRP3 inflammasome is a potential common target of OPPs poisoning and inflammatory reactions in BV2 cells.

Considering that NLRP3 is a possibility target for OPPs poisoning, the interaction between NLRP3 and OPPs is vital. SPR analysis revealed that the affinity of NLRP3-dimethoate was the strongest, while molecular virtual docking revealed a relationship to the exposure of the X1-C(=O)-C(H2)-S-P(=S/-O/-O)-X2 sulfonyl group as sulfur exposure enhanced binding. Affinities of NLRP3-dichlorvos-, -dibrom, and -dimethoate- were stronger, which related to benzene ring or X3-O-P(=O/-O/-O) structure and occurred in combination. Furthermore, the affinities of NLRP3-dimethoate and -paraoxon were stronger, and molecular virtual docking showed that this could be related to exposure to the enhanced binding of -S-, =S, benzene rings, and -O- groups. Affinities of NLRP3-dichlorvos and -dibrom were stronger; the affinity was related to the -(C=CH-), -Cl, or -Br structure and occurred in combination. In terms of structure, OPPs contain hydrophobic groups (benzene rings and hydrocarbon chains) and active groups (-O-, =O, -S-, =S, -Cl, and -Br), in which the benzene ring or hydrocarbon chain with active groups are key structures for interactions with NLRP3 (Israelov et al., 2020; Sharif et al., 2019). The high-frequency residues involved in the hNLRP3-OPPs included Tyr141, Tyr256, Arg268, Gly271, Asp272, Leu273, Ile274, and Cys512, of which Gly271 and Asp272 were the key residues. The common toxicity effector groups of the OPPs were Acc, Hyd, and AtomQ. Common structures of OPPs include abenzene rings, nitrogen/oxygen-containing functional groups (hydrophobic groups), and =O, -O-, or =S (active group) groups; hydrogen bonding and hydrophobic interactions are commonly involved in hNLRP3-OPPs. The common binding mechanisms of proteins and pesticides were analyzed in terms of structure, mode of combination, and toxic effects. A comprehensive analysis and evaluation technique for interactions between proteins and pesticides were established.

5. Conclusions

In conclusion, this study investigated the underlying common mechanisms for the cytotoxic effects of OPPs on BV2 cells and identified potential therapeutic targets for the design of broad-spectrum antitoxins. This is the first study to systematically evaluate the cytotoxicity and activation of NLRP3 inflammasome in BV2 cells induced by various types of OPPs, including paraoxon, dichlorvos, fenthion, dipterex, dibrom, and dimethoate, thus revealing the NLRP3 inflammasome as a potential common target for OPPs poisoning. This NLRP3 inflammasome activation leads to intracellular inflammatory and defense responses, and the associated inflammatory cytokines cause cytotoxic damage. Moreover, this study clarified the common molecular mechanism whereby OPPs activate the NLRP3 inflammasome, revealing common structures, active groups, key residues, hydrogen bonds, interactive areas, IBEI, and toxicity-effector groups. The findings from this study are relevant to the development of specific drug antagonists that could reduce the toxic effects of OPPs poisoning. Consequently, the NLRP3 inflammasome may provide a potential novel target for the development of broad-spectrum antitoxins, which are essential for the MTMC strategy and critical for public health and ecological security.

Supporting Information (SI)

Cell viability, cytotoxicity, expression of the NLRP3 inflammasome, and associated inflammatory cytokine mRNA in BV2 cells treated with OPPs (Figures S1–S3 in Supporting Information S1). Introduction of molecular weight, residue sequences, secondary structure for the main CID chips, and m/z for the NLRP3 LRR (Figure S4 and Table S1 in Supporting Information S1). Two- and three-dimensional structures and Van der Waals' map of OPPs, cryo-EM structure, and key interaction pockets of hNLRP3; two-dimensional interaction information with hydrogen bonding, interaction areas, correlation evaluation, key toxicity-effector groups, and high-frequency groups (≥ 3) of NLRP3-OPPs (Figures S5–S7 and Table S2 in Supporting Information S1).

Conflict of Interest

The authors declare no conflicts of interest relevant to this study.

Data Availability Statement

Data were not used, nor created for this research.

Acknowledgments

This work was financially supported by the National Natural Science Foundation of China [Grants 82273665, 21677030]. We confirm that this work is original, has not been published elsewhere, and is not currently under consideration for publication elsewhere.

References

- Bharate, S., Prins, J. M., George, K. M., & Thompson, C. M. (2010). Thionate versus oxon: Comparison of stability, uptake, and cell toxicity of (¹⁴CH₃O)₂-labeled methyl parathion and methyl paraoxon with SH-SY5Y cells. *Journal of Agricultural and Food Chemistry*, 58(14), 8460–8466. <https://doi.org/10.1021/jf100976v>
- Caruso, G., Fresta, C. G., Grasso, M., Santangelo, R., Lazzarino, G., Lunte, S., & Caraci, F. (2020). Inflammation as the common biological link between depression and cardiovascular diseases: Can carnosine exert a protective role? *Current Medicinal Chemistry*, 27(11), 1782–1800. <https://doi.org/10.2174/0929867326666190712091515>
- Coll, R. C., Robertson, A. A. B., Chae, J. J., Higgins, S. C., Muñoz-Planillo, R., Inserra, M. C., et al. (2015). A small-molecule inhibitor of the NLRP3 inflammasome for the treatment of inflammatory diseases. *Nature Medicine*, 21(3), 248–255. <https://doi.org/10.1038/nm.3806>
- Cowan, F. M., Broomfield, C. A., Stojiljkovic, M. P., & Smith, W. J. (2004). A review of multi-threat medical countermeasures against chemical warfare and terrorism. *Military Medicine*, 169(11), 850–855. <https://doi.org/10.7205/milmed.169.11.850>
- Cowan, F. M., Smith, W. J., Moran, T. S., Paris, M. M., Williams, A. B., & Sciuto, A. M. (2005). Sulfur mustard- and phosgene- increased IL-8 in human small airway cell cultures. *Implications for Medical Countermeasures Against Inhalation Toxicity*.
- Dempsey, C., Rubio Araiz, A., Bryson, K. J., Finucane, O., Larkin, C., Mills, E. L., et al. (2017). Inhibiting the NLRP3 inflammasome with MCC950 promotes non-phlogistic clearance of amyloid-β and cognitive function in APP/PS1 mice. *Brain, Behavior, and Immunity*, 61(1), 306–316. <https://doi.org/10.1016/j.bbi.2016.12.014>
- Duewell, P., Kono, H., Rayner, K. J., Sirois, C. M., Vladimer, G., Bauernfeind, F. G., et al. (2010). NLRP3 inflammasomes are required for atherogenesis and activated by cholesterol crystals. *Nature*, 464(7293), 1357–1361. <https://doi.org/10.1038/nature08938>
- Elliott, E. I., & Sutterwala, F. S. (2015). Initiation and perpetuation of NLRP3 inflammasome activation and assembly. *Immunological Reviews*, 265(1), 35–52. <https://doi.org/10.1111/immr.12286>
- Eychenne, J., Gurioli, L., Damby, D., Belville, C., Schiavi, F., Marceau, G., et al. (2022). Spatial distribution and physicochemical properties of respirable volcanic ash from the 16–17 august 2006 Tungurahua Eruption (Ecuador), and alveolar epithelium response in-vitro. *GeoHealth*, 6(12), e2022GH000680. <https://doi.org/10.1029/2022GH000680>
- Fernandes, L. S., Emerick, G. L., dos Santos, N. A. G., de Paula, E. S., Barbosa, F., & dos Santos, A. C. (2015). In vitro study of the neuropathic potential of the organophosphorus compounds trichlorfon and acephate. *Toxicology in Vitro*, 29(3), 522–528. <https://doi.org/10.1016/j.tiv.2015.01.001>
- Fernandes, L. S., Emerick, G. L., dos Santos, N. A. G., de Paula, E. S., Barbosa, F., & dos Santos, A. C. (2017). High concentration of trichlorfon (1 mM) disrupts axonal cytoskeleton and decreases the expression of plasticity-related proteins in SH-SY5Y cells. *Toxicology in Vitro*, 39, 84–92. <https://doi.org/10.1016/j.tiv.2016.12.003>
- González-González, M., Estévez, J., del Río, E., Vilanova, E., & Sogorb, M. A. (2018). Hydrolyzing activities of phenyl valerate sensitive to organophosphorus compounds paraoxon and mipafox in human neuroblastoma SH-SY5Y cells. *Toxicology*, 406–407, 123–128. <https://doi.org/10.1016/j.tox.2018.07.016>
- Grout, L., Baker, M. G., French, N., & Hales, S. (2020). A review of potential public health impacts associated with the global dairy sector. *GeoHealth*, 4(2), e2019GH000213. <https://doi.org/10.1029/2019GH000213>
- Houzé, P., Hutin, A., Lejay, M., & Baud, F. J. (2019). Comparison of the respiratory toxicity and total cholinesterase activities in dimethyl versus diethyl paraoxon-poisoned rats. *Toxics*, 7(2), 1–23. <https://doi.org/10.3390/toxics7020023>
- Hsu, S. S., Lin, Y. S., Chen, H. C., & Liang, W. Z. (2023). Involvement of oxidative stress-related apoptosis in chlorpyrifos-induced cytotoxicity and the ameliorating potential of the antioxidant vitamin E in human glioblastoma cells. *Environmental Toxicology*, 38(9), 2143–2154. <https://doi.org/10.1002/tox.23850>
- Hu, H. Y., & Yang, L. Q. (2020). Development of enzymatic electrochemical biosensors for organophosphorus pesticide detection. *Journal of Toxicology and Environmental Health-Part B-Critical Reviews*, 56(2), 168–180. <https://doi.org/10.1080/03601234.2020.1853460>
- Israelov, H., Ravid, O., Atrakchi, D., Rand, D., Elhaik, S., Bresler, Y., et al. (2020). Caspase-1 has a critical role in blood-brain barrier injury and its inhibition contributes to multifaceted repair. *Journal of Neuroinflammation*, 17(1), 267. <https://doi.org/10.1186/s12974-020-01927-w>
- Javeres, M. N. L., Habib, R., Laure, N. J., Shah, S. T. A., Valis, M., Kuca, K., & Muhammad Nurulain, S. (2021). Chronic exposure to organophosphates pesticides and risk of metabolic disorder in cohort from Pakistan and Cameroon. *International Journal of Environmental Research and Public Health*, 18(5), 2310. <https://doi.org/10.3390/ijerph18052310>
- Kelly, P., Meade, K. G., & O'Farrelly, C. (2019). Non-canonical inflammasome-mediated IL-1β production by primary endometrial epithelial and stromal fibroblast cells is NLRP3 and caspase-4 dependent. *Frontiers in Immunology*, 10, 102. <https://doi.org/10.3389/fimmu.2019.00102>
- Lamkanfi, M., & Dixit, V. M. (2014). Mechanisms and functions of inflammasomes. *Cell*, 157(5), 1013–1022. <https://doi.org/10.1016/j.cell.2014.04.007>
- Liu, M., Zhang, S. S., Liu, D. N., Yang, Y. L., Wang, Y. H., & Du, G. H. (2021). Chrysoerythrin A attenuates neuroinflammation by down-regulating NLRP3/cleaved caspase-1 signaling pathway in LPS-stimulated mice and BV2 cells. *International Journal of Molecular Sciences*, 22(13), 6799. <https://doi.org/10.3390/IJMS22136799>
- Liu, X., Zhang, Z. B., Ruan, J. B., Pan, Y. D., Magupalli, V. G., Wu, H., & Lieberman, J. (2016). Inflammasome-activated gasdermin D causes pyroptosis by forming membrane pores. *Nature*, 535(7610), 153–158. <https://doi.org/10.1038/nature18629>
- Liu, X. D., Zhang, R., Fan, J. J., Chen, Y., Wang, H. H., Ge, Y. H., et al. (2023). The role of ROS/p38 MAPK/NLRP3 inflammasome cascade in arsenic-induced depression/anxiety-like behaviors of mice. *Ecotoxicology and Environmental Safety*, 261, 115111. <https://doi.org/10.1016/j.ecoenv.2023.115111>
- Long, J. H., Wang, Q., He, H. H., Sui, X., Lin, G. D., Wang, S., et al. (2019). NLRP3 inflammasome activation is involved in trimethyltin-induced neuroinflammation. *Brain Research*, 1718, 186–193. <https://doi.org/10.1016/j.brainres.2019.05.003>
- Man, S. M., & Kanneganti, T. D. (2015). Converging roles of caspases in inflammasome activation, cell death and innate immunity. *Nature Reviews Immunology*, 16(1), 7–21. <https://doi.org/10.1038/nri.2015.7>
- Martín, F., Martínez-García, J. J., Muñoz-García, M., Martínez-Villanueva, M., Noguera-Velasco, J., Andreu, D., et al. (2017). Lytic cell death induced by melittin bypasses pyroptosis but induces NLRP3 inflammasome activation and IL-1β release. *Cell Death & Disease*, 8(8), e2984. <https://doi.org/10.1038/cddis.2017.390>

- Martinon, F., Burns, K., & Tschopp, J. (2002). The inflammasome: A molecular platform triggering activation of inflammatory caspases and processing of proIL- β . *Molecular Cell*, *10*(2), 417–426. [https://doi.org/10.1016/S1097-2765\(02\)00599-3](https://doi.org/10.1016/S1097-2765(02)00599-3)
- Pundir, C. S., Malik, A., & Preety. (2019). Bio-sensing of organophosphorus pesticides: A review. *Biosensors and Bioelectronics*, *140*(6), 5–17. <https://doi.org/10.1016/j.bios.2019.111348>
- Sato, H., Ito, Y., Hanai, C., Nishimura, M., Ueyama, J., & Kamijima, M. (2021). Non-linear model analysis of the relationship between cholinesterase activity in rats exposed to 2, 2-dichlorovinyl dimethylphosphate (dichlorvos) and its metabolite concentrations in urine. *Toxicology*, *450*, 152679. <https://doi.org/10.1016/j.tox.2021.152679>
- Sharif, H., Wang, L., Wang, W. L., Magupalli, V. G., Andreeva, L., Qiao, Q., et al. (2019). Structural mechanism for NEK7-licensed activation of NLRP3 inflammasome. *Nature*, *570*(7761), 338–343. <https://doi.org/10.1038/s41586-019-1295-z>
- Sui, X., Yang, J., Zhang, G. Z., Yuan, X. F., Li, W. H., Long, J. H., et al. (2020). NLRP3 inflammasome inhibition attenuates subacute neurotoxicity induced by acrylamide in vitro and in vivo. *Toxicology*, *432*, 152392. <https://doi.org/10.1016/j.tox.2020.152392>
- Takahashi, M. (2019). Role of NLRP3 inflammasome in cardiac inflammation and remodeling after myocardial infarction. *Biological & Pharmaceutical Bulletin*, *42*(4), 518–523. <https://doi.org/10.1248/bpb.b18-00369>
- Throckmorton, D. C., Volkow, N., Platoff, G., Amaya, K., & Laney, J. (2020). Multi-agency development of medical countermeasures against opioid-induced respiratory depression. *Clinical Pharmacology & Therapeutics*, *109*(3), 576–577. <https://doi.org/10.1002/cpt.2070>
- Voet, S., Guire, C. M., Hagemeyer, N., Martens, A., Schroeder, A., Wieghofer, P., et al. (2018). A20 critically controls microglia activation and inhibits inflammasome-dependent neuroinflammation. *Nature Communications*, *9*(1), 2036. <https://doi.org/10.1038/s41467-018-04376-5>
- Wang, S., He, H. H., Long, J. H., Sui, X., Yang, J., Lin, G. D., et al. (2021). TRPV4 regulates soman-induced status epilepticus and secondary brain injury via NMDA receptor and NLRP3 inflammasome. *Neuroscience Bulletin*, *37*(7), 905–920. <https://doi.org/10.1007/s12264-021-00662-3>
- Wang, X. N., Yang, C. X., Sun, Y. Y., Sui, X., Zhu, T., Wang, Q., et al. (2021). A novel screening strategy of anti-SARS-CoV-2 drugs via blocking interaction between Spike RBD and ACE2. *Environment International*, *147*(7–8), 106361. <https://doi.org/10.1016/j.envint.2020.106361>
- Yang, C. X., Wang, X. N., Ji, Y. J., Ma, T., Zhang, F., Wang, Y. Q., et al. (2019). Photocatalytic degradation of methylene blue with ZnO@C nanocomposites: Kinetics, mechanism, and the inhibition effect on monoamine oxidase A and B. *NanoImpact*, *15*, 100174. <https://doi.org/10.1016/j.impact.2019.100174>
- Yao, J. J., Wang, Z. X., Guo, L. L., Xu, X. X., Liu, L. Q., Xu, L. G., et al. (2020). Advances in immunoassays for organophosphorus and pyrethroid pesticides. *TRAC Trends in Analytical Chemistry*, *131*, 116022. <https://doi.org/10.1016/j.trac.2020.116022>
- Zhang, C., Zhan, J. C., Zhao, M. Y., Dai, H. M., Deng, Y. Y., Zhou, W. J., & Zhao, L. (2019). Protective mechanism of taxifolin for chlorpyrifos neurotoxicity in BV2 cells. *Neurotoxicology*, *74*, 74–80. <https://doi.org/10.1016/j.neuro.2019.05.010>
- Zhang, N., Zhu, L. H., Zhang, R. Z., Zhang, C., Cheng, J. G., Tao, L. M., et al. (2021). Evaluation of toxicological effects of organophosphorus pesticide metabolites on human HepG2 cells. *Environmental Toxicology and Pharmacology*, *88*, 103741. <https://doi.org/10.1016/j.etap.2021.103741>
- Zhu, X. Z., Liu, H. P., Wang, D. Y., Guan, R. L., Zou, Y. K., Li, M., et al. (2023). NLRP3 deficiency protects against hypobaric hypoxia induced neuroinflammation and cognitive dysfunction. *Ecotoxicology and Environmental Safety*, *255*, 114828. <https://doi.org/10.1016/j.ecoenv.2023.114828>
- Zimmer, L. A., Ennis, M., & Shipley, M. T. (1997). Soman-induced seizures rapidly activate astrocytes and microglia in discrete brain regions. *Journal of Comparative Neurology*, *378*(4), 482–492. [https://doi.org/10.1002/\(SICI\)1096-9861\(19970224\)378:4<482::AID-CNE4>3.0.CO](https://doi.org/10.1002/(SICI)1096-9861(19970224)378:4<482::AID-CNE4>3.0.CO)